J Therm Anal Calorim (2010) 101:181–187
DOI 10.1007/s10973-009-0593-3

Thermal analysis of two types of dextran-coated magnetite

Oana Carp · Luminita Patron · Daniela C. Culita · Petru Budrugeac · Marcel Feder · Lucian Diamandescu

Received: 17 June 2009 / Accepted: 28 October 2009 / Published online: 2 December 2009

Abstract The thermal stability of two kinds of dextran-coated magnetite (dextran with molecular weight of 40,000 (Dex40) and 70,000 (Dex70)), obtained by dextran adsorption onto the magnetite surface is investigated in comparison with free dextran in air and argon atmosphere. The thermal behavior of the two free dextran types and corresponding coated magnetites is similar, but atmosphere dependent. The magnetite catalyzes the thermal decomposition of dextran, the adsorbed dextran displaying lower initial decomposition temperatures comparative with the free one in both working atmospheres. The dextran adsorbed onto the magnetite surface decomposes in air through a strong sharp exothermic process up to ~450 °C while in argon atmosphere two endothermic stages are identified, one in the temperature range 160–450 °C and the other at 530–800 °C.

Keywords Dextran-coated magnetite · Thermal analysis · X-Ray diffraction (XRD) · FTIR spectoscopy

O. Carp · L. Patron · D. C. Culita (✉)
Institute of Physical Chemistry "Ilie Murgulescu", Splaiul Independentei, No.202, 060021 Bucharest, Romania
e-mail: danaculita@yahoo.co.uk

P. Budrugeac
ICPE-CA, Splaiul Unirii no.313, Bucharest, Romania

M. Feder · L. Diamandescu
National Institute of Materials Physics, 105 bis Atomistilor Street, P.O. Box. Mg-7, Bucharest-Magurele R-077125, Romania

Introduction

Biocompatible colloids based on nanometric superparamagnetic iron oxide nanoparticles have a wide range of biomedical and diagnostic applications [1–4]. The stability of these colloid suspensions is greatly improved by addition of suitable polymeric dispersants, which can effectively prevent the adhesion of particles during thermal motion. The adsorbed polymer layer should completely cover the particles and should be as closely packed as possible to keep away the iron oxides from a direct contact with blood proteins and phagocytosis-associated receptors.

One of the most common coatings for biocompatible iron oxide-based colloids are derivate of dextran [5–12]. Dextran is a polysaccharide polymer (Fig. 1) composed exclusively of α-D-glucopyranosyl units ($C_6H_{10}O_5$) with varying degrees of length (n) and branching points (usually 1,3 glucosidic linkages).

In aqueous strong alkaline solution, dextran interacts with hydroxyl groups presented on bare magnetite surface. The surface covering leads to formation of aggregates with hydrodynamic diameters between 20 and 150 nm [13].

Several physical and chemical routes have been adopted for synthesis magnetite nanoparticles (powders and films) among which we mention: coprecipitation [14, 15], flow injection synthesis technique [16], water in oil emulsions [17, 18], variants of sol–gel methods [19], hydro/solvothermal processes [20], thermal decomposition of different precursors [21], electrochemical deposition under oxidizing conditions [22], and sonolysis [23], etc.

This study presents the thermal stability of two kinds of dextran-coated magnetite (dextran with molecular weight of 40,000 (Dex40) and 70,000 (Dex70), respectively), obtained by adsorbtion of the polymer (dextran) onto the magnetite surface.

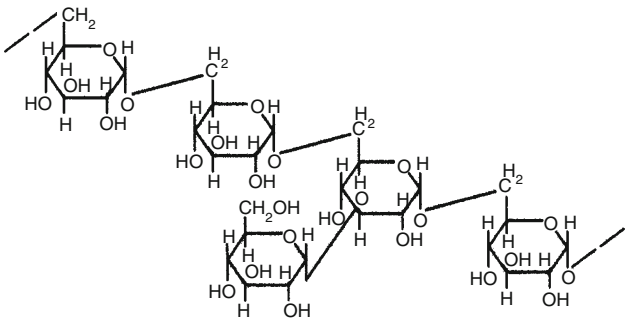

Fig. 1 Molecular formulation of dextran with 1–3 branching

Experimental

Synthesis

A two step synthetic route was used, using $Fe(NO_3)_3{\cdot}9H_2O$ (Merck, p.a.), $FeSO_4{\cdot}7H_2O$ (Merck, p.a.), dextran (molecular weight of 40,000 and 70,000, Fluka, p.a) ammonium hydroxide solution (25%, Reactivul, p.a.) as raw materials. Magnetite (Fe_3O_4) were prepared by coprecipitation of $Fe(NO_3)_3{\cdot}9H_2O$ (4.04 g) and $FeSO_4{\cdot}7H_2O$ (1.38 g), molar ratio = 2:1, by addition of NH_4OH 25% till a pH $\sim$ 10. The black precipatate has been washed several times through decantation. A solution composed of 3 g dextran in 30 ml water (20% dextran) was added under stirring to the resultant magnetite. Subsequently, the dispersion was maintained for 1 h at 80 °C under stirring. The separation of the composite was performed by centrifugation (1 h 15,000 rpm min^{-1}).

Structure investigations

The FTIR investigations were performed on BIO-RAD FTIR 125 type spectrophotometer in KBr pellets and the structure of the as-resulted powders was examined with a DRON X-ray powder diffractometer linked to a data acquisition and processing facility. Cu K_α radiation ($\lambda = 1.540598$ Å) and a graphite monochromator have been used.

Thermal investigations

The thermal investigations were carried under static air, with sample mass about $\sim$20 mg at heating rates of 5 °C min^{-1} on a Netzch thermobalance STA 409 PC/PG type.

Results and discussions

Characterization of dextran-coated magnetite

In order to confirm the modification of magnetite surface with dextran, FTIR spectra of dextran-coated magnetite and free dextran were recorded (Fig. 2). The dextran spectrum (Fig. 2a) exhibits the polysaccharide characteristic absorbtion bands: 3,432 cm^{-1}due to OH stretching, 1,637 cm^{-1} due to water molecule bonding, 2896, 1462, and 1342 cm^{-1} assigned to ν(C–H) and δ(C–H) vibrational modes, 941, 865, and 766 cm^{-1} due to α-glucopyranose ring deformation modes [24]. In dextran-coated magnetite (Fig. 2b), the bands below 1,000 cm^{-1} are overlapped by the Fe–O bands with two maxima at 580 and 419 cm^{-1}. The rest of dextran bands showed no spectral changes upon coating.

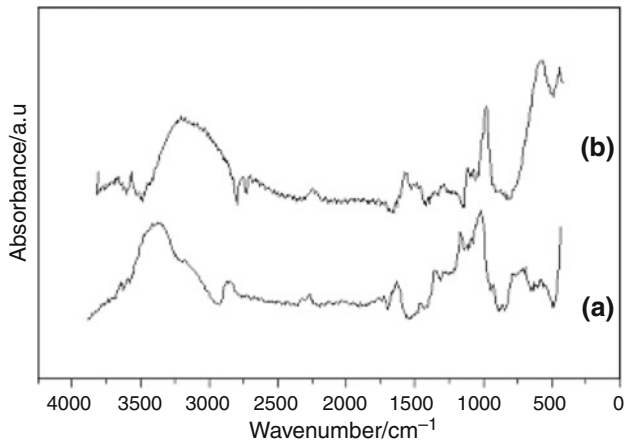

Fig. 2 FTIR spectra of **a** Dex40 and **b** Dex40-coated magnetite

The crystalline structure and phase purity were determined by powder XRD. The diffraction peaks of the dextran-coated magnetite sample are characteristic for a spinel structure of nanoscaled magnetite (Fig. 3).

The crystallite sizes calculated applying the Debye–Scherrer formula based on the half-width of the first five most intense peak of the magnetite phase were in the range 8–10 nm.

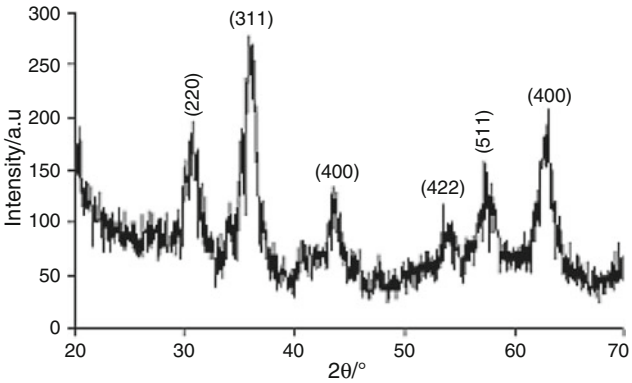

Fig. 3 X-ray diffraction pattern of Dex40-coated magnetite

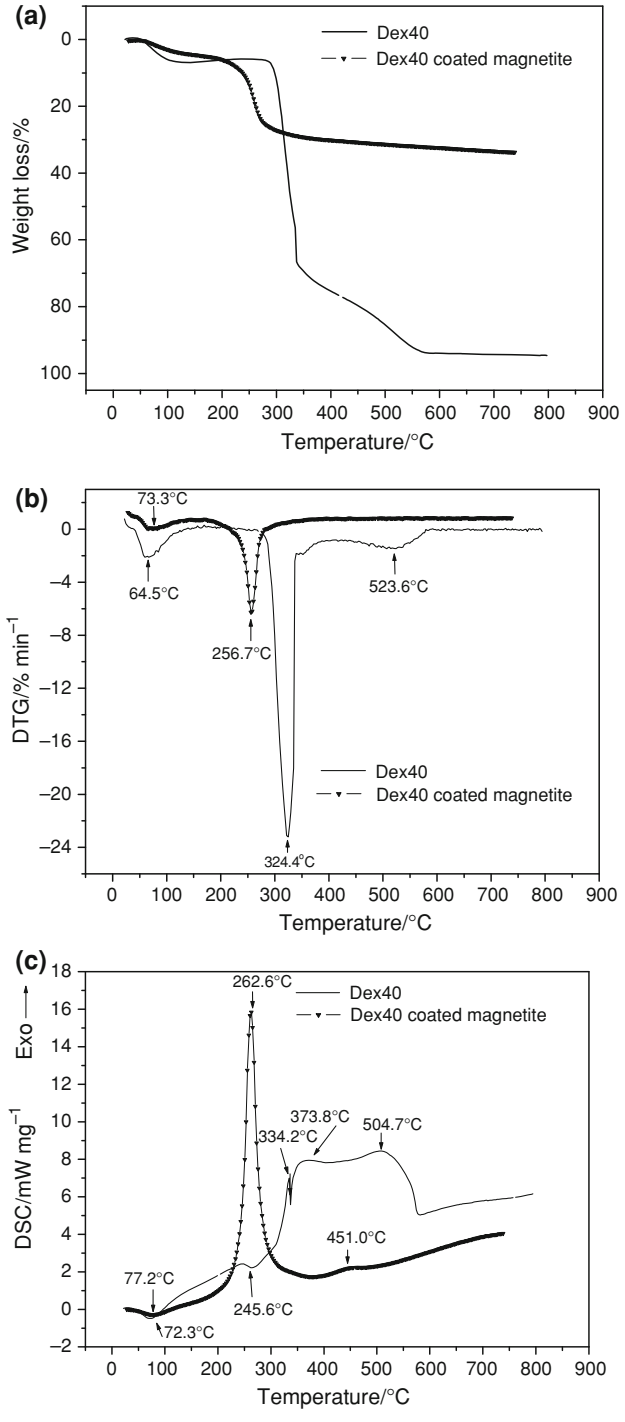

Fig. 4 Thermal decomposition curves of Dex40 and Dex40 coated magnetite (heating rate 5 °C min^{-1}, static air atmosphere): **a** TG; **b** DTG and **c** DSC

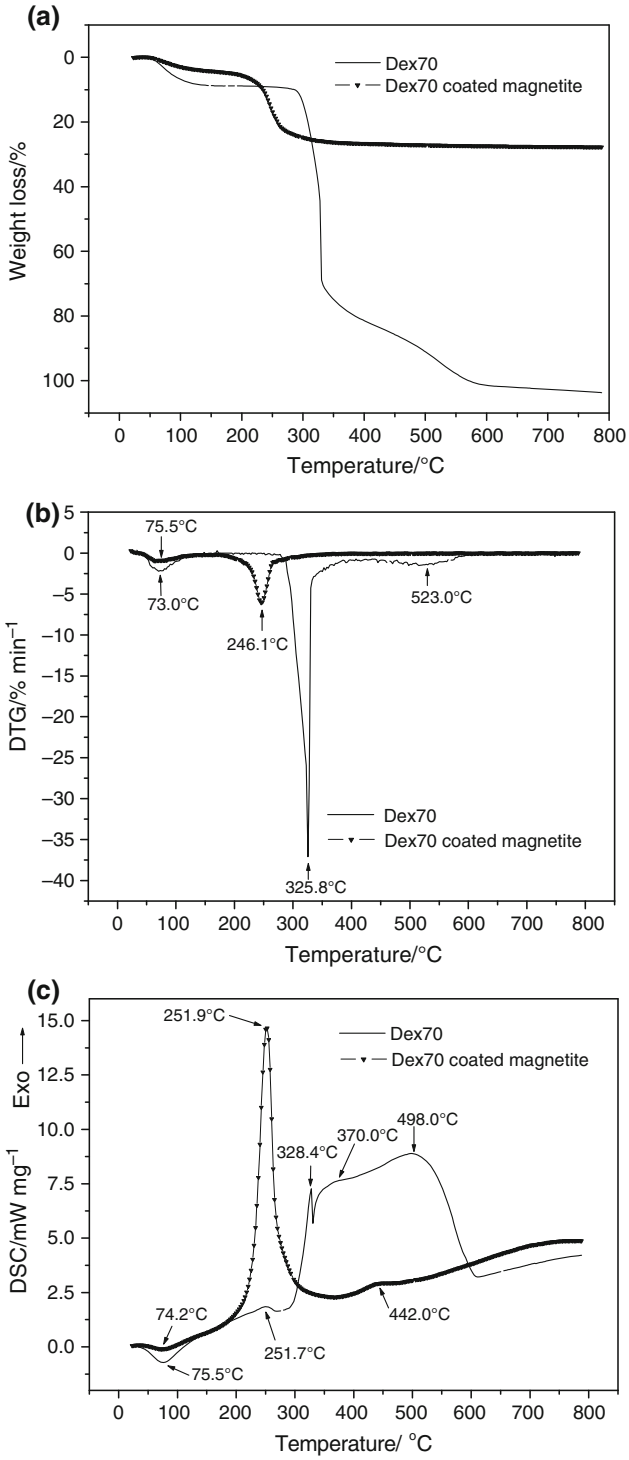

Fig. 5 Thermal decomposition curves of Dex70 and Dex70 coated magnetite (heating rate 5 °C min^{-1}, static air atmosphere): **a** TG; **b** DTG and **c** DSC

Thermal stability of dextran-coated magnetite

The thermal decomposition curves (TG, DTG and DSC) of the dextran-coated magnetites obtained both in air and argon atmosphere are presented in Figs. 4, 5, 6, and 7. The thermal behaviors of the free dextran (Dex40 and Dex70) and corresponding coated magnetites are similar but atmosphere dependent.

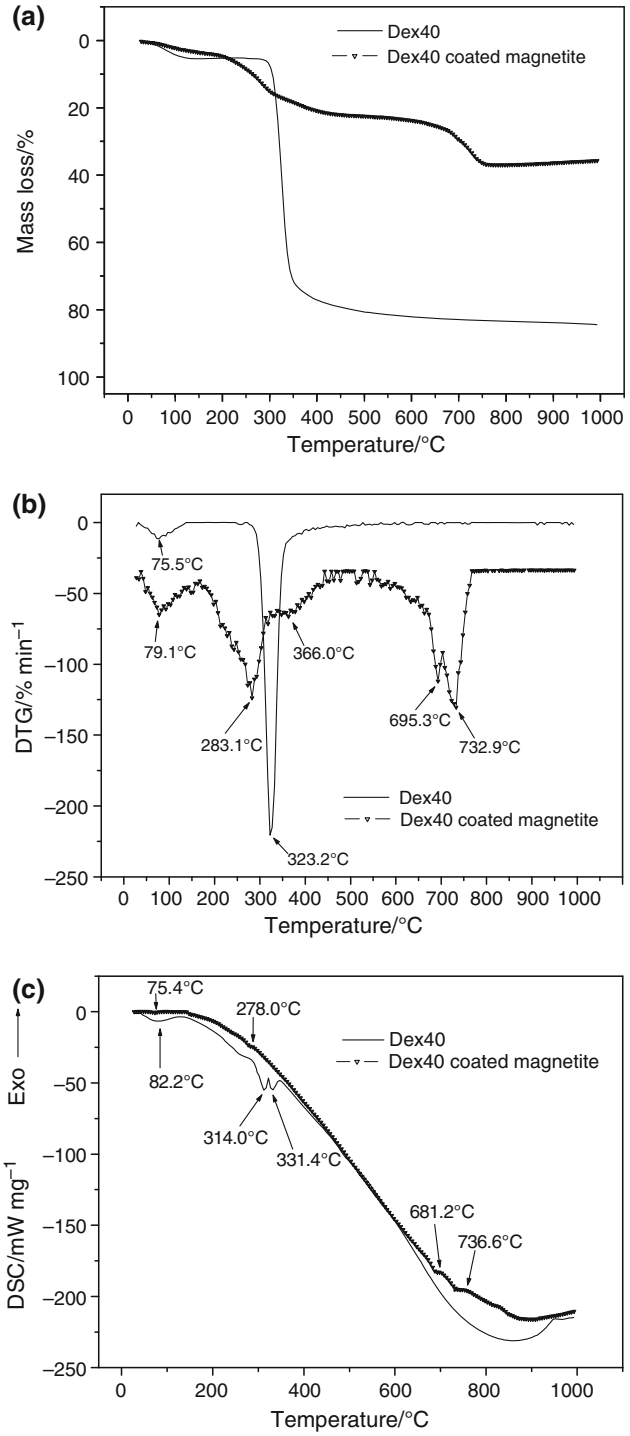

Fig. 6 Thermal decomposition curves of Dex40 and Dex40 coated magnetite (heating rate 5 °C min^{-1}, argon atmosphere): **a** TG; **b** DTG and **c** DSC

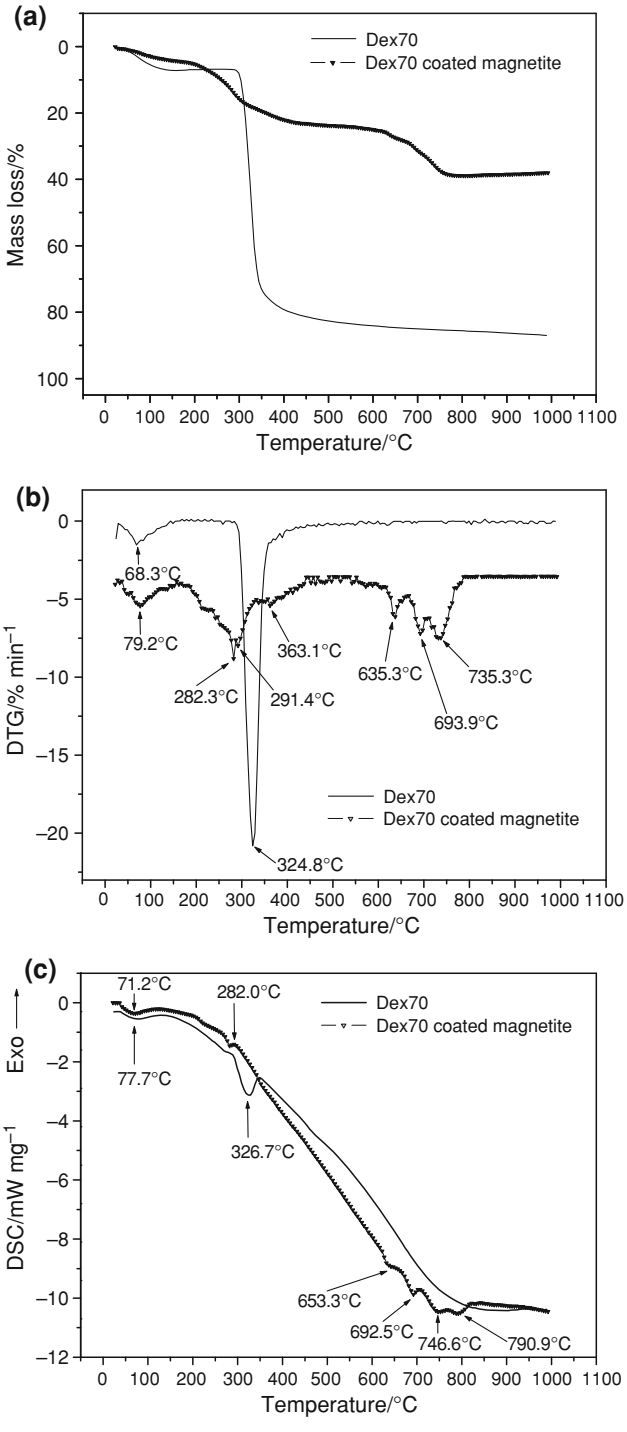

Fig. 7 Thermal decomposition curves of Dex70 and Dex70 coated magnetite (heating rate 5 °C min^{-1}, argon atmosphere): **a** TG; **b** DTG and **c** DSC

In air atmosphere, the free dextran decomposes in three distinctive decomposition stages. The first decomposition step (50.5–155.5 °C/47.0–157.57 °C, mass loss of 7.33 and 8.77% for Dex40/Dex70, respectively) represents the endothermic water evolving. At temperatures higher than 250 °C the breakdown of the organic skeleton starts. A complex degradation process occurs in the temperature range 269.5–427.0 °C/258.0–413.5 °C. The resultant registered mass loss is 73.18%/72.76% (Dex40/Dex70). Three exothermic maxima are evidenced on DSC curves, at 245.6, 334.2, and 373.8 °C (Dex40) and 251.7, 328.4, and

370.0 °C (Dex70). The first of them, is associated with a weak effect, ($\Delta H = 58.58$ J g^{-1}/76.29 J g^{-1}, Dex40/Dex70), the exothermicity of the reaction increases with the increase in decomposition. Rising the temperature, a final exothermic decomposition process occurs (427.0–587.5 °C/413.5–598.2 °C) characterized by a mass loss of 16.94%/19.49% (Dex40/Dex70). It is worth to be mentioned that Dex70 presents also a small gradual mass loss of 1.53% up to 760 °C.

The thermal behavior in air atmosphere of the corresponding coated magnetites presents significant differences. A first weak endothermic process (48.3–156.3 °C/40.5–165.5 °C, mass loss of 4.12%/4.42% for Dex40/Dex70), assigned to adsorbed water elimination is followed by a strong exothermic one (156.3–368.3 °C/165.5–370.5 °C, mass loss of 23.83%/22.15%, Dex40/Dex70) which may be attributed to dextran oxidative degradation. The DSC curves reveal at 451.0 °C/442.0 °C ($\Delta H = 39.28$ J g^{-1}/45.68 J g^{-1}, Dex40/Dex70), an exothermic peak, assigned to γ-$Fe_2O_3 \rightarrow \alpha$-$Fe_2O_3$ transformation. The final mass loss (4.12%/1.13%, Dex40/Dex70) is developed gradually in the temperature range 368.3–750 °C/370.5–780.0 °C, corresponds to the elimination of carbonaceous residue deposited on the magnetite surface.

The magnetite catalyzes the thermal decomposition of dextran in air, the bonded dextran displaying lower decomposition temperatures in comparison with the free one. The initial decomposition temperature decreases with ~100 °C: (269.5 → 156.3 °C/258.0 → 165.5 °C (Dex40/Dex70)), the final with ~220 °C; (587.5 → 368.3 °C/598.2 → 370.5 °C (Dex40/Dex70)), and the one corresponding to the maximum decomposition rate of the decomposition step with maximum weight loss ($T_{DTG\ max}$) with ~70 °C: (324.4 → 256.7 °C/325.8 → 246.1 °C (Dex40/Dex70)). Contrary to the decomposition of free dextran where four exothermic maxima were identified on DSC curve, in the case of coated magnetite a single strong maxima at 262.6 °C/251.9 °C (Dex40/Dex70) is displayed.

The thermal behavior of dextran and corresponding coated magnetites is different in inert (argon) atmosphere comparative with air one.

Two endothermic steps are identified in dextran decomposition on heating till 1,000 °C. The total mass loss is 84.31%/86.97% (Dex40/Dex70) meaning that not all the dextran is decomposed till this temperature. The first step, 42.1–152.0 °C/37.2–139.6 °C (mass loss of 5.34%/7.05%, Dex40/Dex70) represents the water evolving, while the second 262.2–497.2 °C/274.0–434.0 °C (mass loss of 78.96%/71.2%, Dex40/Dex70) the decomposition of the organic compound. A gradual decrease of the mass (6.02%) is registered for Dex70 in the temperature range 434.0–1,000 °C.

The thermal decomposition in argon of the corresponding coated magnetite presents three distinct stages. The decomposition starts with water evolving (43.0–158.8 °C/37.7–152.2 °C, mass loss of 3.71%/4.25%, Dex40/Dex70). The next two corresponds to dextran breakdown and evolving. The first one (168.0–463.0 °C/167.2-452.2 °C, mass losses of 18.49%/19.02%, Dex40/Dex70) is characterized by a single DSC peak (T_{maxDSC} = 278.0 °C and 282.0 °C). As in the case of the air thermal decomposition, the magnetite catalyzes the thermal decomposition of dextran, the adsorbed dextran displaying lower decomposition temperatures comparative with the free one. The initial decomposition temperature of the dextran decreases with ~100 °C: 262.2 → 168.0 °C/274.0 → 167.2 °C (Dex40/Dex70). The second dextran decomposition stage (573.2–773.4 °C/537.2–792.2 °C, mass losses of 14.78%/15.62%, Dex40/Dex70) is characterized by two/four DSC maxima (T_{maxDSC} = 681.2 and 736.6 °C (Dex40) and T_{maxDSC} = 653.3, 692.5, 746.6, and 790.9 °C (Dex70)). At least one of these peaks from each sample may be assigned to the reduction of magnetite to the non-stoichiometric wustite $Fe_{1-x}O$ and/or metallic iron due to the interaction with the evolved gases [25, 26]. A proof for this affirmation is the higher mass losses in argon atmosphere in comparison with air one (in argon mass losses of 36.98%/38.89% were obtained while in air only 27.95%/26.57% (Dex40/Dex70)).

Analyzing the above data the following decomposition mechanism may be advanced:

- the decomposition of free dextran in air commences with the breaking of the polymeric bonds, process which is associated with an endothermic thermal effect. The above process was not evidenced on DSC curves due to the overlapping with the beginning of the degradative oxidation, process coupled with an exothermic effect. As consequence, only a small exothermic effect is registered on the DSC curves at 245.6 °C/251.7 °C (Dex40/Dex70). On further heating, the decomposition of dextran progresses through three exothermic steps.
- in the case of the air thermal decomposition of coated magnetite, the polymeric bond breaking is accompanied by a strong and rapid oxidative degradation of the adsorbed dextran due to the catalytic effect introduced by the iron cations. A catalytic behavior of iron cations toward the degradation of organic coatings, is already reported by the literature in the case of amino acid-coated magnetite [27]. However, unlike the amino acid-coated magnetite, where an abnormal high γ-$Fe_2O_3 \rightarrow \alpha$-$Fe_2O_3$ conversion temperature is registered, (T_{maxDSC} ~ 580 °C), in the

present study hematite formation occurs in the usual temperature range ($T_{maxDSC} \sim 450$ °C).

– two decomposition stages are registered in argon atmosphere for the dextran-coated magnetite while the corresponding anhydrous dextran decomposes only in a single one. Such behavior may have two origins. The first one is the different nature of the dextran-magnetite bonding, a hydrogen bonding, and a chemical one (the formation of a surface complex). The two types of bonding may be formed either during the synthesis process of the coated magnetite or during the heating treatment. Another explanation of this behavior may be a stepped decomposition of the coated dextran. Further investigations are in progress to elucidate this.

Conclusions

The free anhydrous dextran decomposes in air through two distinctive decomposition stages at temperatures up to 600 °C. The decomposition starts with the polymeric bond breaking, followed by oxidative degradation of organic entity. In argon atmosphere only one decomposition stages is identified.

The decomposition of anhydrous-bonded dextran commences at lower temperatures, due to the catalytic effect of magnetite.

The two decomposition stages of the coated dextran in argon atmosphere suggest two types of dextran-magnetite binding, namely a hydrogen and a coordinative bond. Further investigations are in progress to prove this affirmation.

While in air atmosphere the conversion γ-Fe_2O_3 to α-Fe_2O_3 is identified, in argon the magnetite reduction to wurstite and/or metallic iron is advanced to occur.

The proposed synthetic route provides dextran-coated magnetite with bondings between the two components stable up to 150 °C, a useful characteristic for their applications.

References

1. Okassa LN, Marchais H, Douziech-Eyrolles L, Cohen-Jonathan S, Souce M, Dubois P, et al. Development and characterization of sub-micron poly(d, l-lactide-co-glycolide) particles loaded with magnetite/maghemite nanoparticles. Int J Pharm. 2005;302: 187–96.
2. Perez JM, O'Loughin T, Simeone FJ, Weissleder R, Josephson L. DNA-based magnetic nanoparticle assembly acts as a magnetic relaxation nanoswitch allowing screening of DNA-cleaving agents. J Am Chem Soc. 2002;124:2856–7.
3. Kohler N, Fryxell GE, Zhang M. A bifunctional poly(ethylene glycol) silane immobilized on metallic oxide-based nanoparticles for conjugation with cell targeting agents. J Am Chem Soc. 2004; 126:7206–11.
4. Kohler N, Sun C, Fichtenholtz A, Gunn J, Fang C, Zhang M. Methotrexate immobilized poly(ethylene glycol) magnetic nanoparticles for mr imaging and drug delivery. Small. 2006;2: 785–91.
5. Pardol H, Chua-anusorn W, St. Pierre TG, Dobson J. Structural and magnetic properties of nanoscale iron oxide particles synthesized in the presence of dextran or polyvinyl alcohol. J Magn Magn Mater. 2001;225:41–6.
6. Bautista MC, Bomati-Miguel O, Del Puerto Morales M, Serna CJ, Veintemillas-Verdaguer S. Surface characterisation of dextran-coated iron oxide nanoparticles prepared by laser pyrolysis and coprecipitation. J Magn Magn Mater. 2005;293:20–7.
7. Xia Z, Wang G, Tao K, Li J. Preparation of magnetite–dextran microspheres by ultrasonication. J Magn Magn Mater. 2005;293: 182–6.
8. Xu XQ, Shen H, Xu JR, Li XJ, Xiong XM. Core-shell structure and magnetic properties of magnetite magnetic fluids stabilized with dextran. Appl Surf Sci. 2005;252:494–500.
9. Chan HT, Do YY, Huang PL, Chien PL, Chan TS, Liu RS, et al. Preparation and properties of bio-compatible magnetic Fe_3O_4 nanoparticles. J Magn Magn Mater. 2006;304:e415–7.
10. Hai TH, Phuc LH, Dung DTK, Huyen NTL, Long BD, Vinh LK, et al. Iron oxide nanoparticles with biocompatible starch and dextran coatings for biomedicine applications. Adv Nat Sci. 2008;9: 87–92.
11. Morais PC, Silveira LB, Oliveira AC, Santos JG. Initial dynamic susceptibility of biocompatible magnetic fluids. Rev Adv Mater Sci. 2008;18:536–40.
12. Hildebrandt N, Hermsdorf D, Signorell R, Schmitz SA, Diederichsen U. Superparamagnetic iron oxide nanoparticles functionalized with peptides by electrostatic interactions. ARKIVOC 2007;v:79–90.
13. Shen TT, Wiessleder R, Papisov M, Bogdanov AJ, Brady TJ. Monocrystalline iron oxide nanocompounds (MION): physicochemical properties. Magn Reson Med. 1993;29:599–604.
14. Martinez-Mera I, Espinosa ME, Perez-Hernandez R, Arenas-Alatorre J. Synthesis of magnetite (Fe_3O_4) nanoparticles without surfactants at room temperature. Mater Lett. 2007;61:4447–51.
15. Qiu J, Yang R, Li M, Jiang N. Preparation and characterization of porous ultrafine Fe_2O_3 particles. Mater Res Bull. 2005;40: 1968–75.
16. Alvarez GS, Muhammed M, Zagorodni AA. Novel flow injection synthesis of iron oxide nanoparticles with narrow size distribution. Chem Eng Sci. 2006;61:4625–33.
17. Deng Y, Wang L, Yang W, Fu S, Elaissari A. Preparation of magnetic polymeric particles via inverse microemulsion polymerization process. J Magn Magn Mater. 2003;257:69–78.
18. Jia Z, Yujun W, Yangcheng L, Jingyu M, Guangsheng L. In situ preparation of magnetic chitosan/Fe_3O_4 composite nanoparticles in tiny pools of water-in-oil microemulsion. React Funct Polym. 2006;66:1552–8.
19. Dai Z, Meiser F, Möhwald H. Nanoengineering of iron oxide and iron oxide/silica hollow spheres by sequential layering combined with a sol–gel process. J Colloid Interface Sci. 2005;288: 298–300.
20. Mao B, Kang Z, Wang E, Lian S, Gao L, Tian C, et al. Synthesis of magnetite octahedrons from iron powders through a mild hydrothermal method. Mater Res Bull. 2006;41:2226–31.
21. Woo K, Hong J, Ahn JP. Synthesis and surface modification of hydrophobic magnetite to processible magnetite@silica-propylamine. J Magn Magn Mater. 2005;293:177–81.
22. Kahn HR, Petrikowski K. Anisotropic structural and magnetic properties of arrays of $Fe_{26}Ni_{74}$ nanowires electrodeposited in the pores of anodic alumina. J Magn Magn Mater. 2000;215–216: 526–8.

23. Abu Mukh-Qasem R, Gedanken A. Sonochemical synthesis of stable hydrosol of Fe_3O_4 nanoparticles. J Colloid Interface Sci. 2005;284:489–94.
24. Jung CW. Surface properties of superparamagnetic iron oxide MR contrast agents: ferumoxides, ferumoxtran, ferumoxsil. Magn Reson Imaging. 1995;13:675–91.
25. Palnichenko AV, Rossolenko AN, Kopylov VN, Zer'kova II, Aronin AS. Synthesis of wustite nanowires by carbon plasma pulse assisted method. Chem Phys Lett. 2005;410:436–40.
26. Da Costa GM, De Grave E, Vandenberghe PMA. Synthesis and characterization of some iron oxides by sol-gel method. J Solid State Chem. 1994;113:405–12.
27. Patron L, Marinescu G, Culita DC, Diamandescu L, Carp O. Thermal stability of amino acid-(tyrosine and tryptophan) coated magnetites. J Therm Anal Calorim. 2008;91:627–32.